PCCP

Dynamic Article Links ►

Cite this: DOI: 10.1039/c0xx00000x

www.rsc.org/xxxxxx

ARTICLE TYPE

Electron-vibration entanglement in the Born-Oppenheimer description of chemical reactions and spectroscopy

Laura K. McKemmish[ab], Ross H. McKenzie[c], Noel S. Hush[ad], and Jeffrey R. Reimers[ef]*

Received (in XXX, XXX) Xth XXXXXXXXX 20XX, Accepted Xth XXXXXXXXX 20XX

DOI: 10.1039/b000000x

Entanglement is sometimes regarded as the quintessential measure of the quantum nature of a system and its significance for the understanding of coupled electronic and vibrational motions in molecules has been conjectured. Manifested in a spatially localized diabatic basis, such entanglement could possibly be exploited to build qubits in a chemical quantum computer, but manifested in an adiabatic basis it could give new insight into the breakdown of the Born-Oppenheimer (BO) approximation that forms the core of modern chemical understanding. For these purposes, we consider the entanglement associated with individual vibronic eigenfunctions relevant to either low-energy spectroscopic and thermodynamic properties or else chemical reaction processes. In addition, we also consider the development of entanglement during reactive wavepacket dynamics. A two-state single-mode diabatic model that is descriptive of a wide range of chemical phenomena is used for this purpose. Simple expressions are given for specifying electron-vibration entanglement that do not depend on the nature of the wavefunctions considered. The entanglement developed by BO breakdown correlates simply with the diameter of the cusp introduced by the BO approximation, and a hierarchy appears between the various BO-breakdown correction terms, with the first-derivative correction being more important than the second-derivative correction which is more important than the diagonal correction. This simplicity is in stark contrast to the known complexity of thermodynamic, spectroscopic, and kinetic properties. Further, processes poorly treated at the BO level that appear to be adequately treated using the Born-Huang adiabatic approximation are found to have properties that can *only* be described using a non-adiabatic description. For the entanglement developed between diabatic electronic states and the nuclear motion, qualitatively differently behavior is found compared to traditional properties of the density matrix and hence entanglement is shown to provide new and relevant information concerning system properties. For chemical reactions, this type of entanglement simply builds up as the transition-state region is crossed. It is robust to small changes in parameter values and is therefore more attractive for making quantum qubits than is the related fragile ground-state entanglement, provided of course that some means of retaining coherent motion at the transition state can be achieved.

1. Introduction

Entanglement has been extensively researched in recent years and provides an intrinsic measure of the quantum nature of multi-particle systems.[1] The entanglement between two subsystems is zero if their dynamics are independent of one another. The entanglement is large in states that contain non-classical correlations, such as those seen in experiments in which Bell's inequalities are violated. In chemical applications, entanglement has been studied considering e.g., electron-vibration,[2-15] electron-electron,[16-29] vibration-vibration,[30-41] vibration-rotation,[42, 43] rotation-rotation,[44] and electron-spin[45-49] interactions. The primary motivation for this research has been the possibility of exploiting entanglement to fabricate a quantum information processing device with performance properties far in excess of those using classical electronics or optics.[50] A second motivation is to develop more new computational quantum chemistry methods for highly correlated systems.[51] Another less explored reason for considering quantum entanglement within chemical systems is the possibility that it could provide new insight into the quantum world of molecular spectroscopy, thermodynamics, and kinetics, and indeed this aspect is currently receiving significant attention.[6, 30, 31, 52-54] Here we are concerned with what entanglement can tell us about chemical reactions and spectroscopic processes, focusing not only the results that conceivable experiments may yield but also on the understanding of the breakdown of the Born-Oppenheimer (BO) and Born-Huang (BH) adiabatic approximations.[55-58]

The BO approximation leads to the critical concept of molecular potential-energy surfaces obtained considering the electronic motion at fixed nuclear configurations. This approach therefore neglects the effects of nuclear motion on the electronic structure, effects that give rise to unexpected chemical reaction mechanisms and to quantitative changes in molecular vibration frequencies and heats of formation.[55-58] While unexpected reaction mechanisms are of fundamental importance, our recent review[59] indicates that modern computational methods have advanced to the stage that inclusion of this coupling is required

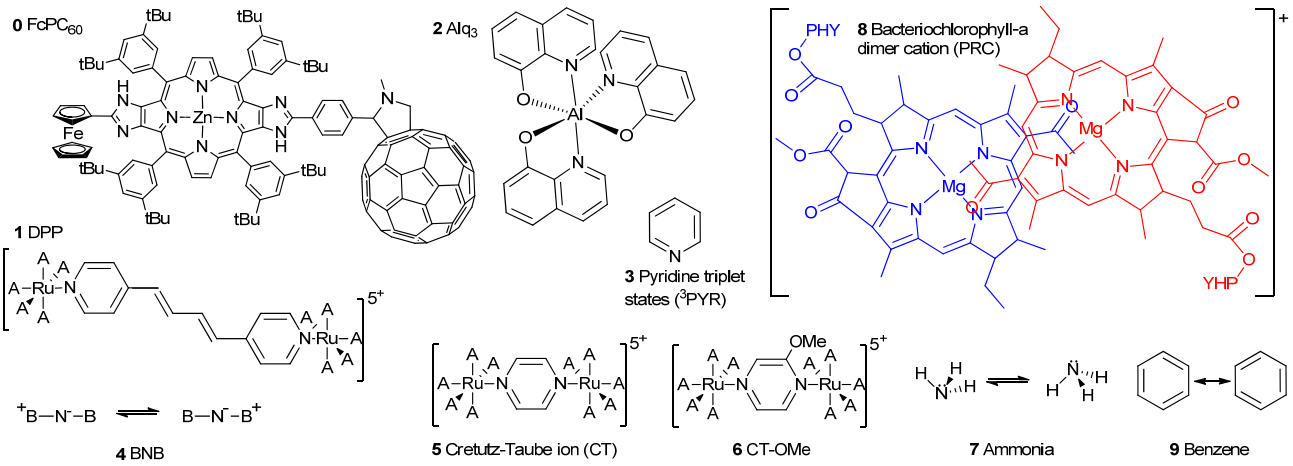

Fig. 1 Some sample molecular systems (see text) with electronic states that can be described using two coupled diabatic potential-energy surfaces. OMe is methoxy, PHY is phytyl; ^{t}Bu is tertiary butyl; A is ammonia; $FcPC_{60}$ is Zinc, [[5,10,16,21-tetrakis[3,5-bis(1,1-dimethylethyl)phenyl]-13-[4-(1',5'-dihydro-1'-methyl-2'*H*-[5,6]fullereno-C_{60}-I_h-[1,9-*c*]pyrrol-2'-yl)phenyl]-1,12-dihydro-23*H*,25*H*-diimidazo[4,5-*b*:4',5'-*l*]porphin-2-yl-κN^{23},κN^{24},κN^{25},κN^{26}]ferrocenato(2-)]-, (*SP*-4-1); Alq3 is *mer*-tris(8-hydroxyquinolinato)aluminum(III); DPP is Ruthenium(5+), decaammine[μ-[4,4'-[(1*E*,3*E*)-1,3-butadiene-1,4-diyl]bis[pyridine-κ*N*]]]di- (9CI).

for the quantitative prediction of observed spectroscopic and thermodynamic properties. Usually the accuracy of the BO approximation is gauged by the magnitude of such errors and by the magnitude of the rate constants of unanticipated reactions. While it is normal to describe unanticipated reactions as being "nonadiabatic", we have recently shown that BH adiabatic potential-energy surfaces typically describe thermally activated processes of this type quite well and hence these reactions should actually only be described as being "non-Born-Oppenheimer" ones.[59] When BH surfaces become inappropriate, dynamics intrinsically involves more than one potential-energy surface and is therefore intrinsically quantum-mechanical.

Regardless, all chemical reactions generate some degree of entanglement between the nuclear and electronic motions, and this effect to some extent always also influences ground-state energetic and spectroscopic properties. Most often the electronic motion can be described in terms of discrete alternative electronic states, while the vibrational motion is universally represented using continuous nuclear vibrational coordinates. The simplest model system is a two-state one-mode vibronic coupling model (sometimes known as the Jahn-Teller $E\otimes B$ Hamiltonian[60] or the two-site Holstein model[61]) in which two diabatic states (representing reactants and products) are coupled through a single harmonic-oscillator vibration: its Hamiltonian **H** is written in terms of spatially localized crude-adiabatic (CA) diabatic states $\phi_L^{CA}(r,Q_0)$ and $\phi_R^{CA}(r,Q_0)$ as

$$\mathbf{H}^{CA}(Q)=\begin{bmatrix} H_{LL}^{CA}(Q) & H_{LR}^{CA}(Q) \\ H_{RL}^{CA}(Q) & H_{RR}^{CA}(Q) \end{bmatrix} \text{ where} \qquad (1)$$

$$H_{LL}^{CA}(Q)=\left\langle \phi_L^{CA}(r,Q_0)\middle|\mathbf{H}\middle|\phi_L^{CA}(r,Q_0)\right\rangle=\frac{\hbar\omega}{2}\left(Q+Q_m\right)^2-\frac{\hbar\omega}{2}\frac{d^2}{dQ^2}$$

$$H_{RR}^{CA}(Q)=\left\langle \phi_R^{CA}(r,Q_0)\middle|\mathbf{H}\middle|\phi_R^{CA}(r,Q_0)\right\rangle=\frac{\hbar\omega}{2}\left(Q-Q_m\right)^2-\frac{\hbar\omega}{2}\frac{d^2}{dQ^2}+E_0$$

$$H_{LR}^{CA}(Q)=\left\langle \phi_L^{CA}(r,Q_0)\middle|\mathbf{H}\middle|\phi_R^{CA}(r,Q_0)\right\rangle=J$$

$$H_{RL}^{CA}(Q)=\left\langle \phi_R^{CA}(r,Q_0)\middle|\mathbf{H}\middle|\phi_L^{CA}(r,Q_0)\right\rangle=J$$

and J is the electronic coupling between the diabatic states, r represents the electronic coordinate, Q represents the chosen (antisymmetric) dimensionless nuclear coordinate, Q_m is a displacement in this coordinate that locates the two harmonic potentials at different nuclear geometries, ω is the vibration frequency of the harmonic diabatic oscillators in the absence of coupling, and E_0 is an energy asymmetry that represents the free-energy change in a chemical reaction. Dimensionless nuclear coordinates are obtained by scaling say normal-mode coordinates by their zero-point displacement length[62] $\sqrt{\hbar/\omega}$.

A very wide range of chemistry is qualitatively depicted by this model. Previously we have used it to detail the failure of the BO approximation for thermodynamic, spectroscopic, and kinetic properties and to determine accurate methods appropriate to a variety of scenarios.[59] We have also used it to outline general considerations concerning the design of a chemical quantum qubit, focusing on the ground-state wavefunction.[2, 3] Here we extend these treatments to consider how entanglement helps to understand breakdown of the BO and BH approximations and how it may be measured during chemical reactions.

To examine the model in detail and demonstrate its applicability, ten model chemical systems **0** – **9** and nine iconic parameter sets **A** – **I** are discussed, see Fig. 1 and Table 1. These model systems include the origin of aromaticity in benzene,[63] symmetry breaking to produce sp^3 hybridization in ammonia,[63, 64] loss of aromaticity in the lowest triplet excited state of pyridine (^{3}PYR),[65] symmetry breaking in BNB, [66] intervalence charge transfer in the Creutz-Taube ion (CT)[67], its orthomethoxy substituted variant CT-OMe[68] and extended bipyridyl form DPP,[69, 70] the photosynthetic bacteriochlorophyll special-pair radical cation from *Rhodobacter sphaeroides*,[71, 72] charge recombination in a ferrocene-porphyrin-fullerene triad photosynthetic model compound ($FcPC_{60}$),[73, 74] and hole transport through the molecular conductor Alq3.[75, 76] They are specified within the parameter space of Eqn. (1) in terms of the three non-trivial variables $2|J|/\lambda$, $\hbar\omega/\Delta E$, and $E_0/\hbar\omega$ which specify the chemical scenario, relative vibrational to electronic energy scale, and relative asymmetry, respectively, where

$$\lambda=2\hbar\omega Q_m^2 \qquad (2)$$

is the reorganization energy and

$$\Delta E=(\lambda^2+4J^2)^{1/2} \qquad (3)$$

Table 1 Estimates (see text) of parameters values for the coupled harmonic potential-energy surfaces for molecular systems **0** – **9** (see Fig. 1) and characteristic points **A** – **I**, along with the evaluated properties at N=1024: Q_c - the cusp diameter (Eqn. (18)), $\Delta\Delta E^{\dagger}$ is the DC to the activation energy (Eqn. (19)); for eigenstates ρ are density-matrix elements (Eqn. (11)) while S is the entanglement (Eqn. (13)) in the BO basis for the lowest vibronic level (0), first-excited level (1), and level at the transition state (T); for wavepackets S_π is the entanglement (BO basis) at $t=\pi/\omega$ whilst κ_{LR} gives the probability of reaction between the diabatic states per period of motion evaluated using the full Hamiltonian (FC) and its BO or BH approximations.

System	$\frac{2\lvert J\rvert}{\lambda}$	$\frac{\hbar\omega}{\Delta E}$	$\frac{E_0}{\hbar\omega}$	Q_c	$\frac{\Delta\Delta E^{\dagger}}{\hbar\omega}$	ρ_0^{+-}	ρ_0^{++}	S_0	ρ_1^{+-}	ρ_1^{++}	S_1	ρ_T^{+-}	ρ_T^{++}	S_T	S_π	κ_{LR}^{FC}	κ_{LR}^{BO}	κ_{LR}^{BH}
0 $FcPC_{60}$	0.029	0.15	-13	0.05	44	0.000	0.000	0.000	0.000	0.000	0.000					0.02[b]	0	0
1 DPP	0.043	0.08	0	0.11	11	0.000	0.000	0.001	0.000	0.000	0.005	0.000	0.037	0.227	0.98	0.08	0.64	0.22
2 Alq3	0.08	0.16	0	0.14	6.3	0.000	0.002	0.020	0.000	0.009	0.076	0.000	0.064	0.344	0.62	0.11	0.68	0.27
3 ^{3}PYR	0.3	0.095	1.3[a]	0.67	0.28	0.013	0.000	0.000	0.013	0.001	0.008	0.007	0.003	0.033	0.19	0.55	0.62	0.56
4 BNB	0.74	0.18	0	1.11	0.10	0.000	0.001	0.010	0.000	0.005	0.041	0.000	0.001	0.010	0.04	0.86	0.92	0.88
5 CT	0.80	0.089	0	1.68	0.04	0.000	0.000	0.002	0.000	0.001	0.006	0.000	0.000	0.002	0.01	0.80	0.83	0.81
6 CT-OMe	0.80	0.089	1.5[a]	1.68	0.04	0.010	0.000	0.000	0.019	0.000	0.001							
7 NH_3	0.80	0.006	0	6.45	0.003	0.000	0.000	0.000	0.000	0.000	0.000	0.000	0.000	0.000	0.00	0.50	0.50	0.50
8 PRC	1.8	0.41	0.6	1.39	0.07	0.020	0.003	0.023	0.040	0.016	0.108							
9 Benzene	3.3	0.010	0	12.6	0.001	0.000	0.000	0.000	0.000	0.000	0.000							
A	0.1	1	0	0.07	25	0.000	0.101	0.471	0.000	0.212	0.746	0.000	0.212	0.746	0.31	0.05	0.76	0.26
B	1	1	0	0.59	0.35	0.000	0.024	0.161	0.000	0.242	0.799							
C	10	1	0	2.23	0.025	0.000	0.005	0.044	0.000	0.332	0.917							
D	0.01	0.1	0	0.02	250	0.000	0.000	0.003	0.000	0.000	0.005	0.000	0.017	0.122	0.81	0.02	0.67	0.02
E	0.1	0.1	0	0.22	2.5	0.000	0.000	0.001	0.000	0.001	0.015	0.000	0.051	0.289	0.86	0.24	0.64	0.39
F	1	0.1	0	1.88	0.035	0.000	0.000	0.002	0.000	0.001	0.007							
G	10	0.1	0	7.05	0.003	0.000	0.000	0.000	0.000	0.000	0.001							
H	0.01	0.0316	0	0.04	79	0.000	0.000	0.000	0.000	0.000	0.000	0.000	0.033	0.209	0.99	0.02	0.61	0.07
I	0.1	0.0316	0	0.40	0.79	0.000	0.000	0.000	0.000	0.000	0.000	0.000	0.006	0.051	0.50	0.45	0.57	0.49

[a] indicated in the figures at the approximate location of $E_0/\hbar\omega$=1.4. [b] inverted region, dynamics at diabatic crossing energy; other approximations yield κ_{LR}^{FD} =0.48, κ_{LR}^{SD} = 0.28, and κ_{LR}^{FD+SD} = 0.05.

is (for E_0 = 0) the adiabatic vertical excitation energy at the geometry of the diabatic minimum (the corresponding adiabatic transition energy at the adiabatic minimum, an easily observable quantity, is simply λ).[59] The values of the parameters used are taken from observed and calculated data,[3, 63, 65-76] as described elsewhere.[3, 59] Values for closed-shell systems are based on our renormalization scheme that maps these essentially multi-state problems onto an effective two-state model.[63] As this mapping is property dependent, we select parameters that relate to the key applications of each particular molecule.

A limitation is that this model includes only a single nuclear coordinate and hence cannot describe Jahn-Teller interactions at conical intersections and are important for in particular photochemistry. Entanglement in these systems is of current interest, however.[2, 10, 11]

Application of the BO approximation[56, 77] to solve for the properties of **H** proceeds by diagonalizing it parametrically as a function of the nuclear coordinate Q to yield the ground-state (-) and excited-state (+) potential-energy surfaces

$$\varepsilon_{\pm}(Q)=\frac{E_0}{2}+\frac{\lambda}{4}+\frac{\hbar\omega}{2}Q^2\pm\left[\left(\frac{E_0}{2}-\hbar\omega Q_m Q\right)^2+4J^2\right]^{1/2} \quad (4)$$

and associated BO electronic wavefunctions

$$\begin{aligned}\left|\phi_-(r,Q)\right\rangle &= a(Q)\left|\phi_L^{CA}(r,Q_0)\right\rangle+b(Q)\left|\phi_R^{CA}(r,Q_0)\right\rangle\\ \left|\phi_+(r,Q)\right\rangle &= -b(Q)\left|\phi_L^{CA}(r,Q_0)\right\rangle+a(Q)\left|\phi_R^{CA}(r,Q_0)\right\rangle\end{aligned} \quad (5)$$

where the mixing coefficients are given by

$$a(Q)=\frac{J}{\left\{J^2+\left[\varepsilon_- -\hbar\omega(Q+Q_m)^2/2\right]^2\right\}^{1/2}},\ \text{and} \quad (6)$$

$$b(Q)=\frac{\varepsilon_- -\hbar\omega(Q+Q_m)^2/2}{\left\{J^2+\left[\varepsilon_- -\hbar\omega(Q+Q_m)^2/2\right]^2\right\}^{1/2}}.$$

However, using these BO wavefunctions as the basis describing the electronic motion, Eqn. (1) may be rewritten *without approximation*[56, 57] as $\mathbf{H}^{BO}(Q)$ where

$$\begin{aligned}H_{ab}^{BO}(Q)&=\left\langle\phi_a^{BO}(r,Q)\middle|\mathbf{H}\middle|\phi_b^{BO}(r,Q)\right\rangle \text{ for } a,b=+,-\text{ and}\\ H_{--}^{BO}(Q)&=\varepsilon_-(Q)+\Delta H^{DC}(Q)-\frac{\hbar\omega}{2}\frac{\partial^2}{\partial Q^2},\\ H_{++}^{BO}(Q)&=\varepsilon_+(Q)+\Delta H^{DC}(Q)-\frac{\hbar\omega}{2}\frac{\partial^2}{\partial Q^2},\\ H_{-+}^{BO}(Q)&=-H_{+-}^{BO}(Q)=\Delta P^{FD}(Q)\frac{\partial}{\partial Q}+\Delta H^{SD}(Q).\end{aligned} \quad (7)$$

Here,

$$\Delta H^{DC}(Q) = \frac{\hbar^2\omega^2\lambda J^2}{4[2J^2 + \hbar\omega\lambda(Q-Q_x)^2]^2},$$
$$\Delta P^{FD}(Q) = \frac{-\hbar^2\omega^2\delta J}{2J^2 + \hbar\omega\lambda(Q-Q_x)^2}, \text{ and} \quad (8)$$
$$\Delta H^{SD}(Q) = \frac{\hbar^3\omega^3\lambda J\delta(Q-Q_x)}{[2J^2 + \hbar\omega\lambda(Q-Q_x)^2]^2}$$

provide the diagonal correction (DC) ΔH^{DC}, first-derivative (nuclear momentum) correction (FD) $\Delta H^{FD} = \Delta P^{FD}(Q)\partial/\partial Q$, and second-derivative (nuclear kinetic energy) correction (SD) ΔH^{SD} to the BO approximation, with

$$Q_x = \frac{E_0}{\lambda} Q_m \quad (9)$$

being the nuclear coordinate at which the two CA states intersect.[59] Solving Eqn. (6) retaining all three correction terms provides a numerically exact solution to the original model Hamiltonian, while neglecting one or more of the correction terms generates approximate methodologies; the BO approximation corresponds to neglecting all three corrections whilst the BH approximation retains only DC, ignoring the FD and SD surface-hopping contributions.

The primary observable consequences of entanglement in quantum systems stem from the results of making measurements for one of the observable properties of the system.[1] If entanglement is present then such measurements also reveal unexpected information concerning other aspects of the system. Therefore the nature of the measurement must always be specified when considering entanglement. Measurement projects a quantum wavefunction onto some basis, and calculations of this entanglement must mimic this. This computational aspect is unusual as most observable properties arise independent of the basis in which the calculations are performed. While unitary transformations of basis sets do not modify entanglement,[1] Eqn. (6) is non-unitary owing to its parametric dependence on the nuclear coordinate. Hence the entanglement measured in the diabatic basis will be different to that measured in the BO basis.

Detectors could conceivably be built that project wavefunctions onto a spatially localized diabatic basis, providing possibilities for the experimental exploitation of entanglement in some quantum information technology.[4-9] Previously, we have described this entanglement within the ground-state wavefunction in detail,[2, 3] estimating its usefulness for quantum computation.[3] Here, we extend this work to look at the entanglement developed during chemical reactions.

In addition, we also focus on the entanglement developed in the BO basis. As the BO approximation is a mathematical construct, it is difficult to envisage an experiment that could perform the related measurements. However, owing to the fundamental importance of the BO approximation to the conceptual framework of chemistry, understanding this entanglement could yield conceptual advances. Indeed, this possibility is of considerable current interest,[6, 30, 31, 52, 53] as is the possibility of examining vibration-vibration entanglement resulting from BO breakdown.[30, 31] Classical molecular dynamics simulations based on the BO approximation do not allow for entanglement and so these measures may provide a robust method for accessing the suitability of molecular dynamics applications to chemical kinetics and spectroscopy.

2. Methods

Entanglement in the CA or BO bases is calculated using harmonic-oscillator basis sets[62] $|\chi_i(Q)\rangle$ centred at Q = 0 to describe the vibrational motions on each electronic basis state. This basis set is truncated at N functions per state. Calculations in the CA basis are mostly rapidly convergent and we use a typically grossly excessive value of N = 256 functions. However, scenarios involving small cusp diameters lead to extremely large basis-set requirements for the evaluation of BO breakdown and we report results that are either converged or nearly so using at N = 1024 functions.[59] The vibronic matrix elements in the CA basis are determined analytically whilst those in the BO basis are evaluated numerically.[59, 62] Diagonalization of the vibronic interaction matrices then yields (numerically equivalent for $N = \infty$) energy eigenvalues ε_j and eigenvectors $|\psi_j(r,Q)\rangle$

$$\begin{aligned} &= \sum_{i=1}^{N} C_{ij}^{-} |\phi_{-}(r,Q)\rangle |\chi_i^{-}(Q)\rangle + C_{ij}^{+} |\phi_{+}(r,Q)\rangle |\chi_i^{+}(Q)\rangle \\ &= \sum_{i=1}^{N} C_{ij}^{L} |\phi_L^{CA}(r,Q_0)\rangle |\chi_i^{L}(Q)\rangle + C_{ij}^{R} |\phi_R^{CA}(r,Q_0)\rangle |\chi_i^{R}(Q)\rangle \end{aligned} \quad (10)$$

For not just eigenstates but for any general time-dependent wavefunction expressed in one of these forms, the entanglement is calculated by first determining the appropriate reduced electronic density for wavefunction j[1, 3]

$$\boldsymbol{\rho}_j = \begin{bmatrix} \rho_j^{--} & \rho_j^{-+} \\ \rho_j^{-+} & \rho_j^{++} \end{bmatrix} \text{ or } \boldsymbol{\rho}_j^{CA} = \begin{bmatrix} \rho_j^{LL} & \rho_j^{LR} \\ \rho_j^{LR} & \rho_j^{RR} \end{bmatrix}, \quad (11)$$

where

$$\rho_j^{ab} = \sum_{i=1}^{N} C_{ij}^{a} C_{ij}^{b}, \quad (12)$$

where either $a,b \in \{+,-\}$ or $a,b \in \{\mathrm{L},\mathrm{R}\}$. In terms the von Neumann entropy, the entanglement present is then given by[1]

$$S_j = -\mathrm{Tr}(\boldsymbol{\rho}_j \log_2 \boldsymbol{\rho}_j) \text{ or } S_j^{CA} = -\mathrm{Tr}(\boldsymbol{\rho}_j^{CA} \log_2 \boldsymbol{\rho}_j^{CA}). \quad (13)$$

Note that it is also possible to obtain this entanglement equivalently by an analogous procedure utilizing instead the reduced vibrational density.[3]

The entanglement developed as a function of time during the motion of wavepackets is obtained by expressing the initial wavepacket as a Gaussian distribution of nuclear position probability on a BO surface as say

$$|\Psi(r,Q;0)\rangle = \pi^{-1/4} \exp\left[-(Q+Q_0)^2/2\right] |\phi_{-}^{BO}(r,Q)\rangle \quad (14)$$

where Q_0 is the initial location of the centre of the wavepacket. This is then projected onto the 2N vibronic eigenstates of the BO electronic Hamiltonian (Eqn. (7)) as

$$|\Psi(r,Q;t)\rangle = \sum_{j=1}^{2N} d_j(t) |\psi_j(r,Q)\rangle. \quad (15)$$

It's quantum dynamics is evaluated analytically using

$$d_j(t) = d_j(0) \exp\left(-i\varepsilon_j t/\hbar\right). \quad (16)$$

The wavefunction is then rewritten into the form of Eqn. (10) and the entanglement determined.

3. Results

a. Entanglement in the ground-vibronic state, first-excited vibronic state, and transition-state adiabatic wavefunctions

The energy of the ground-vibronic wavefunction is important in determining e.g. heats of reaction, while this and the energy of the next-lowest vibronic level determine the lowest spectroscopic

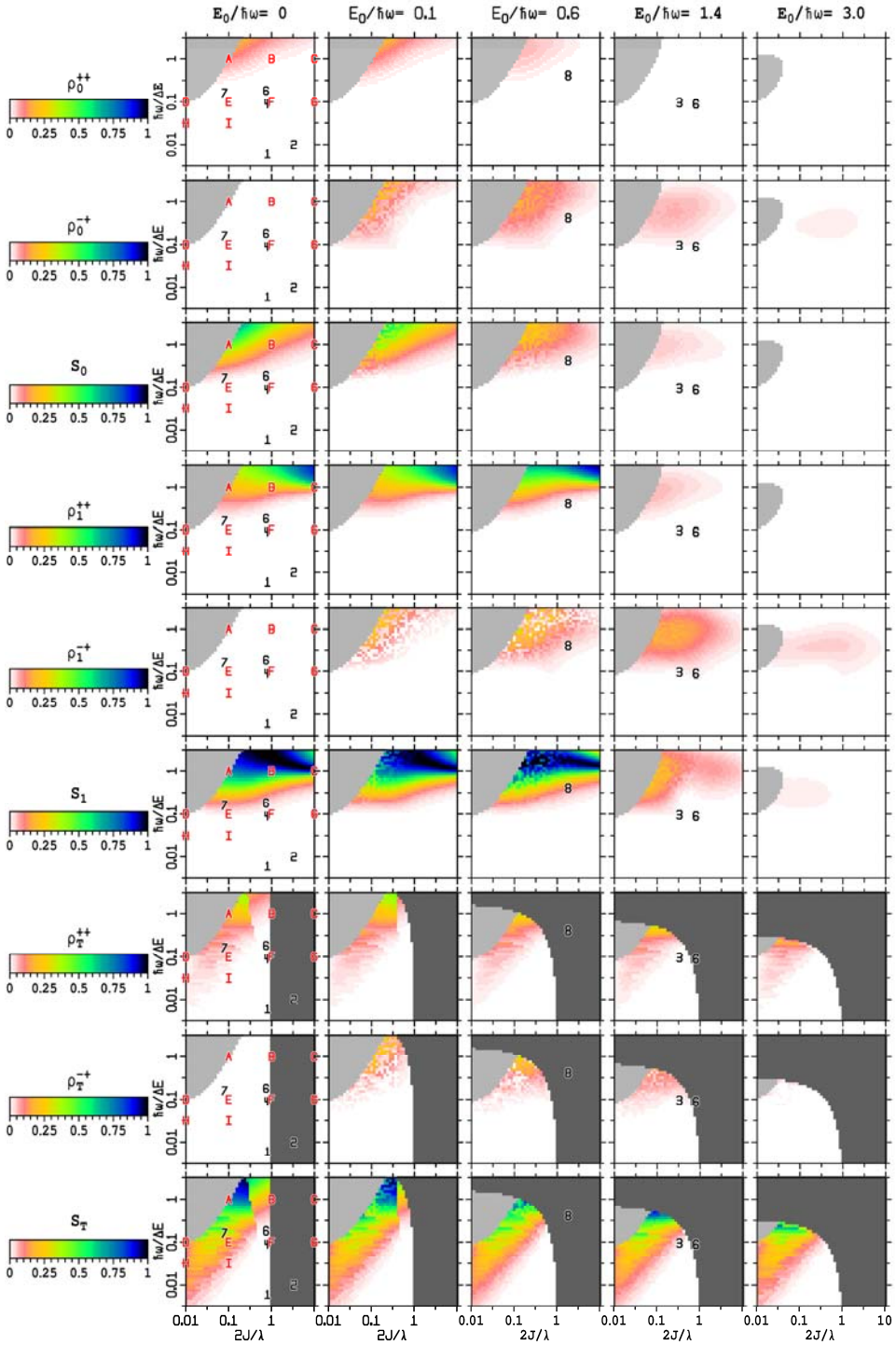

Fig. 2 Measures of BO wavefunction mixing for the lowest (0) , first-excited (1), and near transition-state (T) vibronic eigenfunctions of the two-state one-mode model: ρ^{-+} - electronic off-diagonal density, ρ^{++} - electronic excited-state density, *S* - entanglement. Model compounds **1**-**9** and points **A**-**I** are indicated; regions with poor numerical convergence are shown in light grey whilst those without a transition state are in dark grey.

transition energy; other properties of these wavefunctions determine transition moments, Stark susceptibilities, etc.. Here we use entanglement to quantify how quantum in nature these eigenfunctions appear within the BO approximation, a result that pertains to the suitability of using just a single adiabatic electronic state to describe system properties.

Alternative commonly used measures for intrinsic quantum nature include the values of the excited-state density ρ^{++} and the off-diagonal density-matrix element ρ^{-+} themselves, and we compare these measures with the associated entanglement in Fig. 2 and Table 1 for three eigenfunctions of the two-state one-mode

model. These eigenfunctions are: the lowest vibronic energy level (0), the first vibronic excited-state (1), and the eigenstate closest in energy to that of the transition state, when one exists. The ground-state BO surface has no transition state whenever[59]

$$\left(\frac{\hbar\omega}{\Delta E}\right)^2\left(\frac{E_0}{\hbar\omega}\right)^2 \geq \left[1-\left(\frac{2|J|}{\lambda}\right)^{2/3}\right]^3\left[1+\left(\frac{2J}{\lambda}\right)^2\right]. \qquad (17)$$

These regions are indicated by dark-grey shading in the figure.

If classical molecular dynamics on the ground-state adiabatic surface is to be reliable, then all three measures of the wavefunction ρ^{++}, ρ^{-+}, and *S* need to be very small whereas all three measure approach unity in the worst-possible cases. Fig. 2 shows that the individual density components ρ^{++} and ρ^{-+} sometimes have similar qualitative dependencies on the model parameters $2|J|/\lambda$, $\hbar\omega/\Delta E$, and $E_0/\hbar\omega$ whereas sometimes they behave quite differently. The entanglement, which from Eqn. (13) is sensitive to both density components, indicates that classical mechanics would be unsuitable whether or not this feature can be attributed to ρ^{++} and/or ρ^{-+}. It therefore provides a general way for the interpretation of complex data, the entanglement being only a single number independent of the level of complexity in the density matrix.

All of the sample molecules **0** – **9** have vibrational to electronic energy spacing ratios $\hbar\omega/\Delta E < 0.5$. Above this value molecules would most likely be Jahn-Teller active and therefore must be depicted using at least two nuclear coordinates to incorporate important additional effects not included in our model. Nevertheless, from Fig. 2 it can be seen that adiabatic models fail significantly only in this case. Small but significant entanglement is found in the ground-state wavefunction for the iconic molecule **4** (BNB) (*S*=0.01) as well as for the technologically relevant systems **2** (Alq3) (*S*=0.02) and **8** (PRC) (*S*=0.02), however.

BO entanglement within the first excited vibronic level is generally larger than that in the ground vibronic level as excited states access the cusp region more, this entanglement growing towards unity for systems in the Jahn-Teller region. From Table 1, the largest entanglement calculated for any of the model compounds is 0.11 for **8** (PRC), with entanglement becoming important also for **1** (DPP), **3** (^{3}PYR), and **5** CT. The entanglement at the transition state is quite large for the weakly coupled electron-transfer molecules **1** (DPP) and **2** (Alq3), reaching 0.23 and 0.34, respectively. As the electronic coupling becomes weaker, the entanglement increases indicating enhanced failure of the BO approximation. This is no surprise as non-adiabatic computational methods are almost always used to study such processes; rather it is surprising just how little entanglement is actually developed for quite small values of $2|J|/\lambda$ of order 0.04 – 0.08, and that entanglement decreases significantly as the vibration frequency falls. Reduced vibration frequencies would occur e.g. if an electron transfer process was most strongly coupled to low-frequency solvent modes rather than to intramolecular vibrations.

b. Entanglement in the ground-state and transition-state diabatic wavefunctions

As conceived experiments could make measurements in a spatially localized basis that closely resembles the diabatic states L and R, entanglement in this basis is of fundamental interest for quantum information applications. Previously[3] we have mapped out this entanglement for the ground-state vibronic wavefunction and shown that it correlates poorly with the diabatic-state densities but is closely related to whether or not the vibrational density profile of the ground vibronic level is bimodal (i.e., has two local maxima at different geometries and an intermediary local minimum). In Fig. 3 some of these critical results are reproduced where they are compared to the off-diagonal density profile ρ_0^{LR} and extended to describe the vibronic wavefunction closest in energy to the transition state.

Concerning the ground-state wavefunction, the new results indicate that while the entanglement appears to correlate with the off-diagonal density at $E_0 = 0$, no general correlation is found. Hence, the entanglement provides a different perspective on the system properties than is obtained using conventional representations of the density. The bimodality of the density may be assessed as done previously[3] using the exact wavefunction but in addition it is possible to use the BO approximation to calculate it, with the two approaches compared in Fig. 3. Good agreement is generally obtained, indicating that BO calculations can provide significant physical insight into this measureable entanglement property; they overestimate bimodality for small values of $2|J|/\lambda$. However, as in this region the local minimum in the BO density profile is very shallow and is removed by the addition of a small amount of excited-state character into the wavefunction. Bimodality of the density is a property of general interest that is somewhat analogous to technologically relevant quantum phase transitions.[78]

The results shown in Fig. 3 for the density and entanglement of the vibronic level closest in energy to the BO transition state have a striated nature owing to the changing nature of this level with the system parameters. However, it is clear that the entanglement near the transition state is in general much larger than that found for the lowest vibronic level, as one would expect. Also, the entanglement in the lowest vibronic level is large only for $E_0 = 0$ and is very fragile,[3] often decreasing dramatically for very small asymmetries $E_0/\hbar\omega \sim 0.01$, whereas the entanglement at the transition state is robust, decreasing slowly with increasing asymmetry. While we have argued that the fragility of the ground-level entanglement would effectively prevent the construction of robust chemical qubits,[3] qubit operation based on much higher energy levels would in principle be possible. However, such qubits would suffer from the alternate problem that wavefunctions at high energy decohere much more rapidly than do low-energy ones. From Fig. 3, the entanglement at the transition state appears to be maximal near the line

$$0.35 = Q_c = \frac{2|J|}{\lambda}Q_m = \frac{2|J|}{\sqrt{2\hbar\omega\lambda}} \approx 0.16\left(\frac{2|J|}{\lambda}\right)^{3/4}\left(\frac{\hbar\omega}{\Delta E}\right)^{-1/2} \qquad (18)$$

where Q_c is the diameter of the cusp that appears during the solution of the BO equations,[59] being large only in its vicinity as reactions become more exothermic or endothermic. It is curious that the maximum entanglement at the transition state in the diabatic basis occurs along the dividing line that separates regions of the parameter space in which the DC correction to the BO approximation is small ($Q_c > 0.35$, bottom-right corner of the $2|J|/\lambda$ vs. $\hbar\omega/\Delta E$ parameter space) and where it is large ($Q_c < 0.35$, top-left corner).[59] The values of the cusp diameter for the sample molecules and systems are given in Table 1.

c. Entanglement between vibrations and adiabatic states developed during chemical reactions

In Figs. 2 and 3, the properties of the closest eigenstate to the

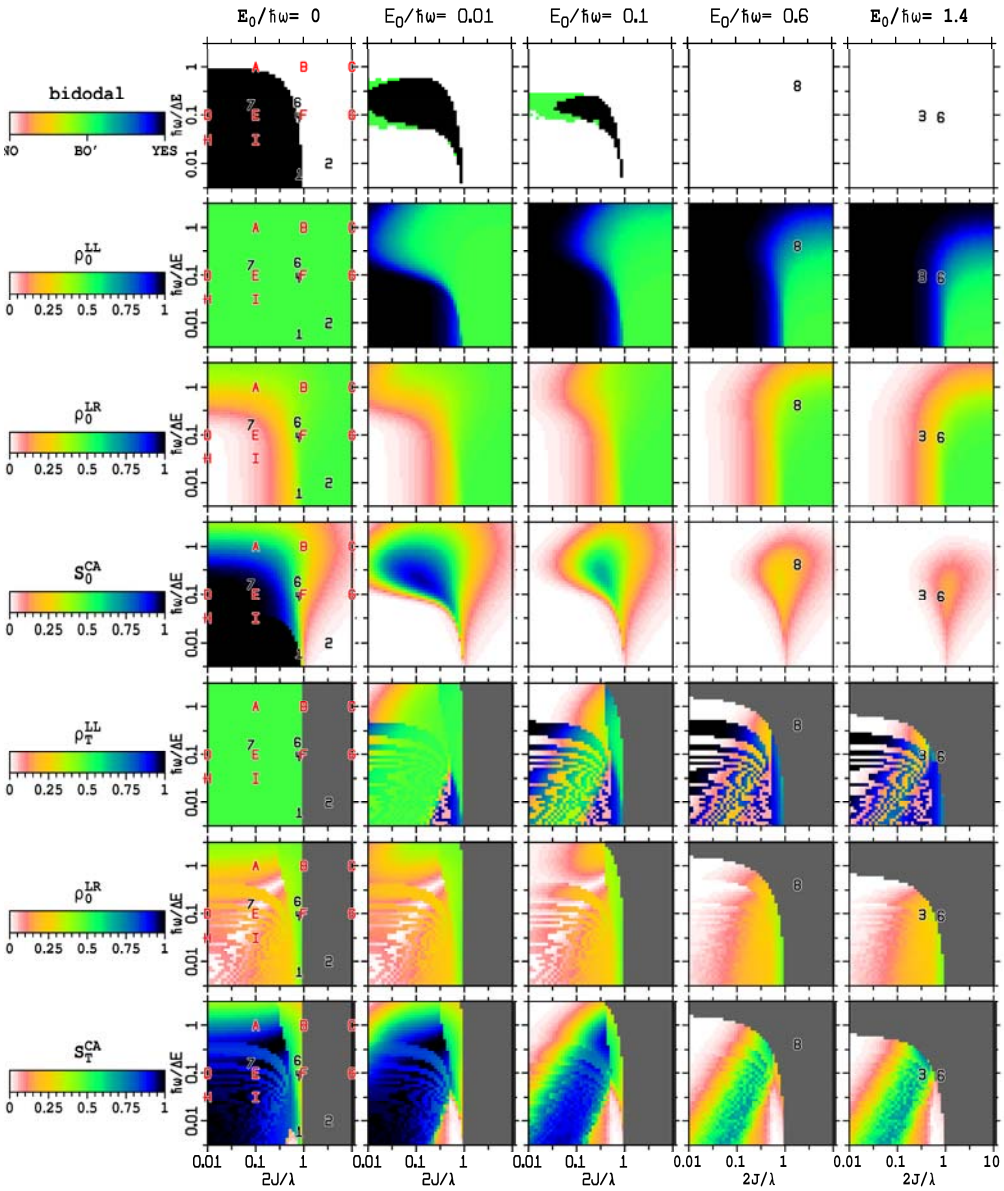

Fig. 3 Measures of diabatic (CA) wavefunction mixing for the lowest (0) and near transition-state (T) vibronic eigenfunctions of the two-state one-mode model: ρ^{LR} - electronic off-diagonal density, ρ^{LL} - diabatic state density, S - entanglement. Model compounds **1**-**9** and points **A**-**I** are indicated, see Table 1; regions without a transition state are shown in dark grey.

transition state were considered. However, few experiments proceed utilizing such eigenstates as chemical dynamics usually involves a non-stationary initial state that converts into a product state when it decoheres. A useful model for general processes of this type is the dynamics of an initial coherent-state wavepacket. Such wavepackets move coherently (i.e., their centres evolve according to classical mechanics and they do not change shape) in the absence of coupling, J=0. Fig. 4 shows how this dynamics is perceived by calculations based on the BO approximation and the ensuing entanglement that develops between the vibrational motion and BO electronic states.

Ten sample trajectories are considered, examining the 4 parameter values **D**, **E**, **H**, and **I** as well as molecule **0** ($FcPC_{60}$) and **5** (CT). These trajectories are run at either the energy of the transition state (top frames of Fig. 4), modelling thermal reactions over a transition-state barrier, or at four times this energy for **D**, **E**, and **I** or at the value of the reorganization energy for **5** (bottom frames), modelling high-energy photochemical processes. While the low-energy trajectories should provide good qualitative descriptions of the properties of all model chemical systems considered, the high-energy trajectories depict *only part* of the story as these reactions actually proceed over conical intersections and require at least two nuclear coordinates to properly describe.

All trajectories start on one of the BO adiabatic potential-energy surfaces which we assume to adequately represent a realistic initial state on one of the diabatic surfaces. The dynamics is followed for one period of the coherent motion that would be produced if J=0. After this time a fraction κ_{LR} of the wavepacket gets transferred to the other diabatic state. We assume that the decoherence processes that would trap the products act infinitely quickly and hence ignore any subsequent

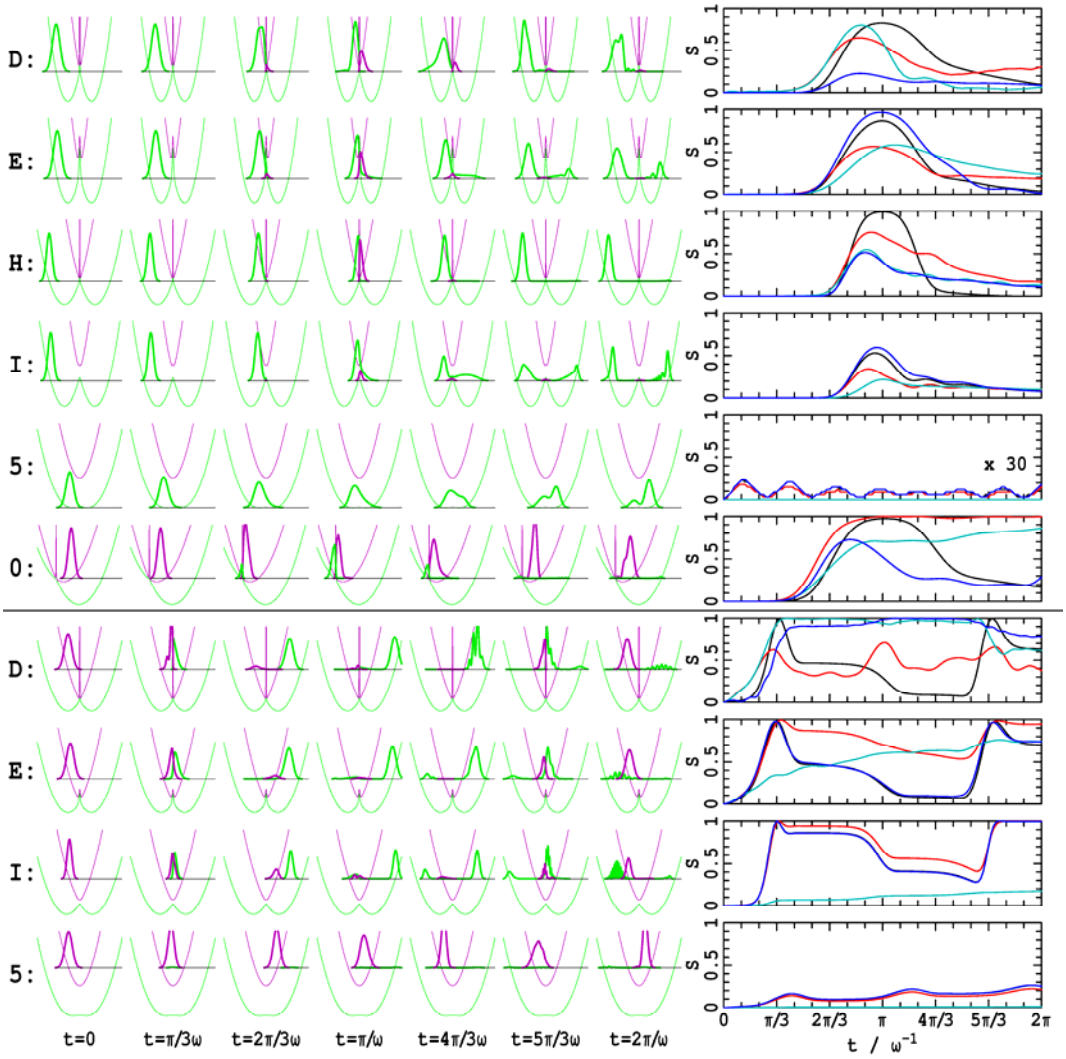

Fig. 4 Quantum dynamics of a Gaussian wavepacket starting at either the energy of the transition state (upper frames, mimicking thermal reactions) or four-times the energy of the diabatic crossover (lower frames, related to photochemical processes) for characteristic points **A**, **E**, **H**, and **I** (see Table 1) as well as for molecules **0** ($FcPC_{60}$) at **5** (CT). The left frames show the BH adiabatic potential-energy surfaces (green- ground state, purple- excited state) and the wavepacket's vibrational density resolved onto these states, while the right frames show the development of the entanglement in the BO basis using: black- exact dynamics, red- DS-only approximation, blue- SD-only approximation, and cyan- FD+SD approximation.

dynamics, dynamics that would in reality be controlled by interference effects and be very sensitive to the number of modes considered in the analysis. This is a useful approximation that is central to the Landau-Zener[79, 80] and other models of chemical reaction kinetics.[81] Table 1 shows this fraction for all of the sample molecules and data points that support transition states, evaluated using the BO approximation, the BH approximation, and the full calculation (FC) embodying all three BO-breakdown corrections. In the region of the parameter space for which the BO approximation works well, all three methods predict similar reaction yields, but otherwise large differences appear.

Fig. 4 shows the time evolution of the wavepacket's vibrational density, projected onto either the BO ground state (in green) or excited state (in purple). In addition, the BH adiabatic potential-energy surfaces are also shown. These surfaces differ from the more usual BO ones $\varepsilon_{\pm}(Q)$ in that the correction term $\Delta H^{DC}(Q)$ is also added. This correction adds a sharp spike of diameter Q_c and height

$$\Delta\Delta E^{\dagger} = \frac{\hbar\omega}{8Q_c^2} = \frac{(\hbar\omega)^2\lambda}{16J^2} = \frac{\hbar\omega}{4}\left(\frac{\hbar\omega}{\lambda}\right)\left(\frac{2J}{\lambda}\right)^{-2} \qquad (19)$$

near the transition state,[59] see Table 1.

Fig. 4 also shows the entanglement between the BO electronic states and the vibrations that develops during the trajectories. Not only is the actual entanglement shown stemming from the full calculation utilizing all 3 BO-breakdown corrections but also the entanglement stemming from three approximate calculations: inclusion of only the FD correction, as is commonly applied in most calculations of BO breakdown, inclusion of only the SD correction, and inclusion of FD+SD only. The BO and BH approximations themselves are adiabatic and hence generate no entanglement; the entanglements from the full calculations at the critical time of $t = \pi / \omega$ are shown in Table 1.

Table 2 presents a qualitative summary of the effects seen in Fig. 4, indicating the minimum number of BO correction terms that must be included in order to obtain reasonable predictions of entanglement for the depicted chemical scenarios. These results

Table 2. Summary of the BO correction terms that must be included in the Hamiltonian in order to model realistically reaction rates, energetics, spectroscopy, or the entanglement in the BO basis.

Systems	Energy[a]	Q_c	Reaction rate described by	Entanglement described by
A	low	0.07	[needs $N > 1024$ basis functions]	
1,**2**,**B**,**D**,**E**,**H**	low	<0.6	[c]	BO+DC+FD+SD
3,**4**,**5**,**8**,**I**	low	0.6-1.7	[c]	BO+FD+SD
6,**7**,**9**,**C**,**F**,**G**	low	>1.6	[c]	BO+FD
D	med.	0.02	BO+DC	BO+DC+FD+SD
E	med.	0.22	BO+DC+FD+SD	BO+DC+FD+SD
H	med.	0.04	BO+DC+FD+SD	BO+DC+FD+SD
I	med.	0.40	BO+DC	BO+FD+SD
5	med.	1.68	BO	BO+FD
0	med.[b]	0.06	BO+DC+FD+SD	BO+DC+FD+SD
D	high	0.02	BO+DC+FD+SD	BO+DC+FD+SD
E	high	0.22	BO+FD+SD	BO+FD+SD
I	high	0.40	BO+FD	BO+FD+SD
5	high	1.68	BO+FD	BO+FD

[a] low- the lowest-energy spectroscopic transition, med.- thermal reactions at the transition-state energy, high- photochemical reactions with significant excess energy. [b] inverted region. [c] lowest-level energies and spectroscopy require: BO only for **3**,**7**,**9**,**G**,**H**,**I** with $\hbar\omega / \Delta E < 0.1$, BO+DC for **0**,**1**,**2**,**4**,**5**,**6**,**D**,**E**,**F** with $0.08 < \hbar\omega / \Delta E < 0.18$, and BO_DC+FD+SD for **8**,**B**,**C**with $\hbar\omega / \Delta E > 0.6$.

are combined with those for the entanglement of the low-energy eigenfunctions discussed earlier. They are also compared to previously obtained[59] qualitative conclusions concerning the importance of the three BO breakdown corrections deduced by examining calculated spectroscopic properties and reaction rates. In this table, properties of ground-vibronic-level wavefunctions are labelled *low*-energy ones, thermal reaction rates over a transition state are labelled *medium*-energy properties, whilst rates for photochemical processes with significant excess energy are labelled *high*-energy properties.

Run at the transition-state energy (medium energy), the trajectory for sample point **D** ($2J / \lambda = 0.01$, $\hbar\omega / \Delta E = 0.1$, $E_0 = 0$) shown in Fig. 4 depicts a classic weakly coupled symmetric electron-transfer reaction in the "non-adiabatic" regime. The initial wavepacket moves coherently until it strikes the transition-state region at which it is mostly reflected by the large BH transition-state energy spike of height $\Delta\Delta E^{\dagger} = 250\,\hbar\omega$ (Table 1), but a small component does undergo surface hopping to the BO excited state induced by the FD and SD terms. The fraction that surface hops quickly hops back, however, and becomes reunited with the directly reflected wavepacket. Using just N=1024 basis functions per state is slightly inadequate for this trajectory, however, as by $t = 2\pi / \omega$ a near complete reformation of the original wavepacket is actually expected (see the converged propagation in the CA basis shown later in Fig. 5) whereas the displayed function is slightly distorted. Table 1 shows that the BH approximation correctly predict that just 2% of the wavepacket reacts during this process and hence the reaction perhaps should not be described as "non-adiabatic", instead it appears to be just "non-Born-Oppenheimer". Indeed, in Table 2 this reaction is depicted as being well described using the BH (i.e., BO+DC) approximation. However, Fig. 4 shows that the entanglement becomes very large amidst the encounter with the transition state, reaching $S = 0.81$ at $t = \pi / \omega$. The BH adiabatic approximation completely misses this entanglement and so whilst some properties of the system may be well described using an adiabatic method, this is not a general result. Table 2 indicates that all BO breakdown corrections (BO+DC+FD+SD) must be included in order to adequately calculate the entanglement for this system as all approximate methods that include surface hopping in some form but neglect the DC correction lead to relatively poor descriptions of the entanglement.

Trajectory **E** is a variant of this trajectory for which the coupling is increased an order of magnitude to $2J / \lambda = 0.1$. Now $\Delta\Delta E^{\dagger}$ is just 2.5 $\hbar\omega$ and so the DC correction no longer acts to reflect the incoming wavepacket. The product yield increases to 24% but now all correction terms must be used for the calculation of both the yield and the entanglement (Table 2). Interestingly, the entanglement profiles are somewhat insensitive to the change in the coupling. Trajectory **H** also involves a much reduced BH barrier correction of $\Delta\Delta E^{\dagger} = 79\,\hbar\omega$ so that direct reflection is also reduced, arising here through reduction of the vibration frequency to $\hbar\omega / \Delta E = 0.0316$. While the reaction yield remains at just 2% owing to the increased effects of surface hopping, the entanglement profiles look qualitatively similar. To complete this series, trajectory **I** evokes both changes simultaneously to make the BH barrier insignificant and also induce a band gap between the BO (and BH) surfaces). Now the BO approximation provides a useful description of the dynamics but the DC correction should still be included. The manifested entanglement is reduced by nearly half and is adequately modeled using only the surface-hopping FD+SD. In addition we also show dynamics for **5** (CT), a strongly coupled system showing a very shallow double well that the bimodality plot in Fig. 3 reveals does not support zero-point vibration. The BO approximation works well for this molecule, with any deviations, including the buildup of a small amount of entanglement that can be adequately described using the FD correction alone.

Also shown in Fig. 4 is the dynamics of a wavepacket mimicking photochemical charge recombination in **0** ($FcPC_{60}$), a medium-energy reaction that occurs in the Marcus inverted region where there is no transition state. While the three BO-breakdown corrections act in qualitatively different manners in the normal and inverted regions[59, 82] the effect of the BH correction is still to block reaction while the entanglement profiles look qualitatively similar. The major qualitative difference between reactions in the inverted region and those in the normal region is that entanglement is essential only for reactions in the inverted region, but this feature is not reflected in the entanglement profiles themselves.

Finally, Fig. 4 shows trajectories for scenarios **D**, **E**, and **I** run at high energy as would be appropriate for many photochemical reactions. The BH barrier still reflects the incoming wavepacket when the barrier is high enough, but the effect is much less than for thermal trajectories owing to the presence of the excess wavepacket energy. Even for scenario **D** for which $\Delta\Delta E^{\dagger} = 250\,\hbar\omega$ and the excess energy above the BO transition state is only 7.3 $\hbar\omega$, the amount of reflection remains modest. This indicates that surface hopping before the barrier is accessed and/or tunnelling through the barrier remains significant throughout a large region of the parameter space when the reactant velocity is high. Like reactions in the inverted region, these photochemical reactions only occur via surface hopping and so only occur when there is entanglement and so from a kinetics perspective they behave fundamentally differently[59, 82] to medium-energy thermal reactions, as is clear from Table 2. The behaviour of the entanglement is analogous to that found for thermal trajectories that do not critically require entanglement, however, becoming large only when the wavepacket encounters the transition state and being attenuated only by the buildup of a significant band gap between the adiabatic states.

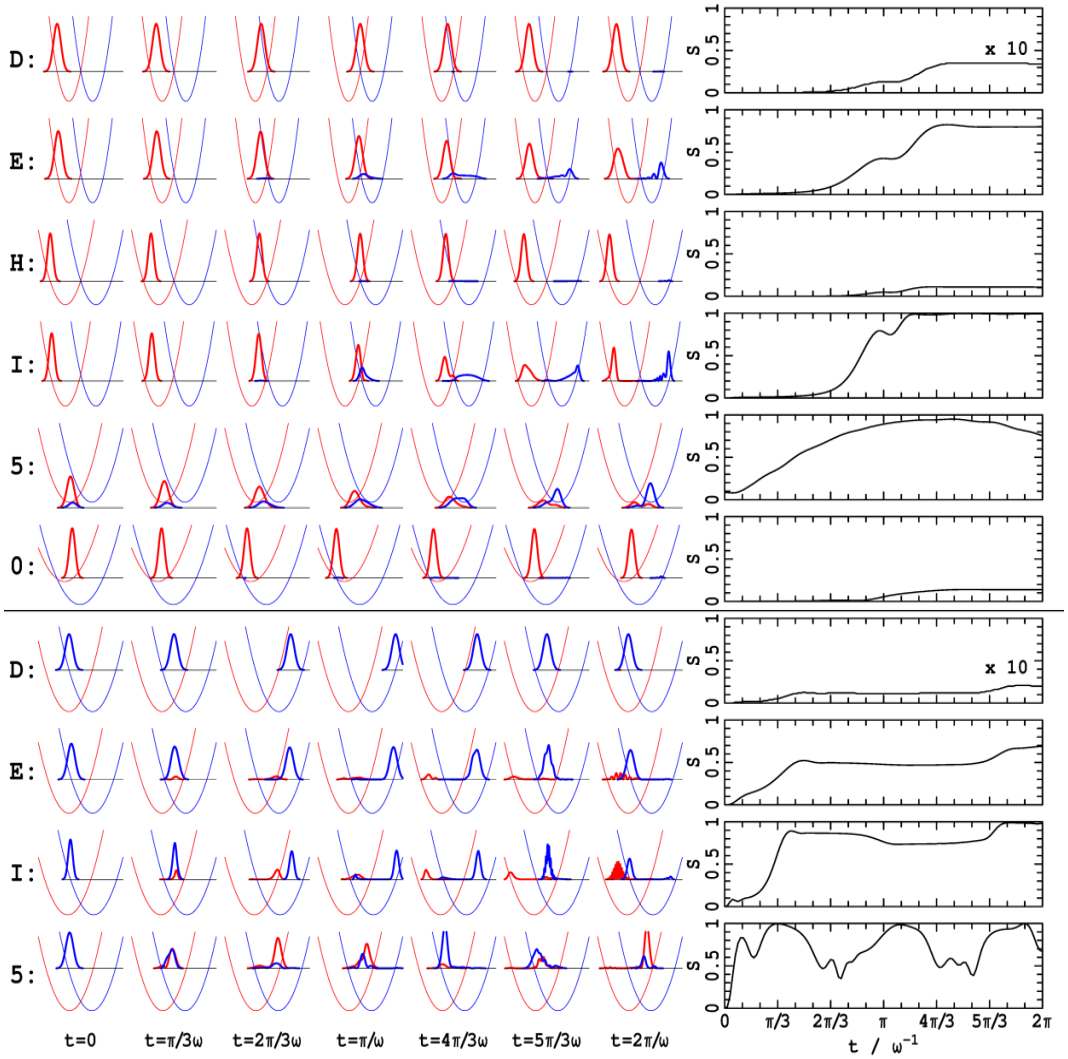

Fig. 5 Quantum dynamics of a Gaussian wavepacket starting at either the energy of the transition state (upper frames, mimicking thermal reactions) or four-times the energy of the diabatic crossover (lower frames, related to photochemical processes) for characteristic points **A**, **E**, **H**, and **I** (see Table 1) as well as for molecules **0** ($FcPC_{60}$) at **5** (CT). The left frames show the diabatic potential-energy surfaces (red- L state, blue- R state) and the wavepacket's vibrational density resolved onto these states, while the right frames show the development of entanglement in the CA basis.

Table 2 indicates that the BO entanglement manifested in low-energy eigenfunctions and in reactive trajectories follows a simple pattern controlled by the value of the cusp diameter. When $Q_C > 1.6$, use of only the FD correction is sufficient to model it whereas for $Q_C < 0.2$-0.6 all 3 corrections are required, with just the two surface-hopping corrections FD+SD sufficing in the intermediary region. This picture conforms to basic expectations of the effects of BO breakdown based on the known relationships linking the 3 correction terms: DC is the square of the FD terms whilst SD is its derivative.[81{Reimers, 2015 #657, 83, 84} This simplicity is lost when complex observed phenomena are considered, however. Table 2 shows that the lowest spectroscopic transition energy scales not with the cusp diameter but rather with the vibrational to electronic energy ratio $\hbar\omega / \Delta E$. It also shows that chemical reaction rates scale in this expected fashion only for high-energy photochemical reactions for which the DC correction acts in a specific but unimportant way, whereas for medium-energy thermal reactions, DC plays the critical role. Indeed, for large cusp diameters great than ca. 1, the BO approximation itself is adequate to describe kinetics, BO+DC is required for slightly smaller values, values of order $0.04 < Q_C < 0.2$ need all terms BO+DC+FD+SD, yet even smaller values require just BO+DC again.

d. Entanglement between vibrations and diabatic states developed during chemical reactions

In Fig. 5 is shown the same dynamics as in Fig. 4 but this time the wavepacket is shown projected onto the diabatic electronic states and the entanglement is that as manifest in the CA basis. This dynamics comes from the direct use of Eqn. (1) rather than through the introduction of the BO approximation.

For thermal trajectories at the transition-state energy, essentially coherent dynamics of the initial diabatic wavepacket is obtained for the weakly coupled electron-transfer-type system **D**, with diabatic surface hopping increasing (i.e., the BO approximation becomes more apt) as the cusp diameter increases through systems **E**, **H**, **I**, and **5**. The (in principle measureable) entanglement in the diabatic basis increases accordingly, becoming large for cases **E**, **I**, and **5**. Unlike entanglement in the BO basis, this entanglement remains after the wavepacket leaves

the transition-state region. Reactions in the inverted region generate little entanglement, and high-energy photochemical reactions have properties analogous to the associated thermal ones. Note that the repetitive encounters of the wavepacket with the transition state followed for the low-reaction-rate high-energy collisions simply increase the entanglement. In the CA basis all reactions require entanglement to proceed but these calculations suggest that the rate of production of this entanglement does correlate in some way with the rate constant for the reaction between the reactant and product diabatic surfaces.

4. Conclusions

Using a simple model representing many chemical kinetic and spectroscopic properties, we have looked at the entanglement that develops between adiabatic electronic states and the vibrational motion as well as that which develops between diabatic electronic states and the vibrational motion. These are done both for the lowest energy eigenstates of the system and for eigenstates near the energy of the transition state, as well as for the dynamics of wavepackets undergoing chemical reactions at the energy of the transition state or well above. Sometimes the processes considered behave such that they could be adequately modeled using classical adiabatic force fields and sometimes they instead appear to be highly quantum in nature. As entanglement is now often regarded as being the quintessential descriptor of quantum effects[1] we investigate the correlation between the two sets of phenomena. This is done bearing in mind more traditional descriptors of the quantum nature of a system, the nature of the associated diagonal and off-diagonal elements of the density matrix. Does entanglement tell us different information than comes from the traditional descriptors? Does the entanglement tell us anything about how to calculate key experimentally measured properties such as reaction yields?

No general answers to these basic questions emerge as findings are context sensitive. For single eigenfunctions of either low energy or the energy of the transition state, the entanglement tells little new information concerning BO breakdown beyond what is apparent from consideration of more traditional density-matrix descriptors. For reactive trajectories performed using BO methods, the entanglement becomes large whenever the transition-state region is encountered and the BO approximation fails, as one would expect. However, the amount of effort required to accurately calculate this entanglement scales in a very simple way with the diameter of the cusp induced by the BO approximation. For small cusp diameter, only the leading term in the expansion of the exact Hamiltonian in terms of BO states, the FD term, is important. As the diameter decreases and BO breakdown becomes more profound, first the SD term must additionally be included and then finally the DC term. This orderly progressive failure of the BO approximation is not reflected in the calculation of other properties such as chemical reaction rates for which each individual term gains special significance depending on the nature of the specific rate process being considered.[59] Indeed, orderly failure is in general not expected for mathematical systems with cusps according to general considerations of the Catastrophe theory.[85-87] Thus entanglement does tell us important information concerning the structure of BO breakdown but conversely it cannot be used to determine how to calculate general system properties. However, it provides an easy to calculate measure of the quality of a wavefunction that is different to the energy-based criteria often used to judge wavefunction convergence, a measure that may relate more to the requirements of other wavefunction properties such as transition and dipole moments.

Alternatively, for entanglement perceived between diabatic states and the nuclear motion for both low-energy eigenfunctions and eigenfunctions near the transition state, the profile of the entanglement throughout the parameter space of the chemical model is distinctly different to those for the individual density-matrix elements considered in traditional analyses of chemical properties. Hence consideration of the entanglement reveals information in a unique and useable way. This is of particular significance as this type of entanglement may in principle be utilized in some quantum information technology. Further, the entanglement developed within reactive wavepackets for both thermal and photochemical reactions behaves in a simple way that could also possibly lead to technological exploitation.

Acknowledgments

We thank the Australian Research Council Discovery Projects scheme for funding, National Computational Infrastructure (NCI) for providing computational resources, and Profs. Meredith Jordan and Timothy Schmidt for helpful discussions.

Notes and references

a: School of Chemistry, The University of Sydney, Sydney, NSW 2006 Australia
b: Department of Physics and Astronomy, University College London, Gower Street, London WC1E 6BT UK
c: School of Mathematics and Physics, The University of Queensland, Brisbane, QLD 4072 Australia
d: School of Molecular Biosciences, The University of Sydney, Sydney, NSW 2006 Australia
e: International Centre for Quantum and Molecular Structure, College of Sciences, Shanghai University, Shanghai 200444 China; Tel: 61 293514468; E-mail: Jeffrey.Reimers@uts.edu.au
f: School of Mathematical and Physical Sciences, University of Technology Sydney, NSW 2007 Australia

1. M. A. Nielsen and I. L. Chuang, *Quantum Computation and Quantum Information*, Cambridge University Press, New York, 2000.
2. A. P. Hines, C. M. Dawson, R. H. McKenzie and G. J. Milburn, *Phys. Rev. A*, 2004, **70**, 022303.
3. L. K. McKemmish, R. H. McKenzie, N. S. Hush and J. R. Reimers, *J. Chem. Phys.*, 2011, **135**, 244110/1.
4. A. J. Ferguson, P. A. Cain, D. A. Williams and G. A. D. Briggs, *Phys. Rev. A*, 2002, **65**, 034303.
5. S. Y. Cho and R. H. McKenzie, *Phys. Rev. A*, 2006, **73**, 012109.
6. R. Englman and T. Vértesi, *J. Chem. Phys.*, 2006, **125**, 064102.
7. R. Englman, *Phys. Lett. A*, 2007, **367**, 345.
8. T. Vértesi and R. Englman, *Phys. Rev. A*, 2007, **75**, 022315.
9. D. Wahyu Utami and A. A. Clerk, *Phys. Rev. A*, 2008, **78**, 042323.
10. B. Kinshuk and G. Gautam, *J. Phys. B: At., Mol. Opt. Phys.*, 2012, **45**, 045102.
11. T. Dereli, Y. Gul, P. Forn-Diaz and O. E. Mustecaplioglu, *Phys. Rev. A: At., Mol., Opt. Phys.*, 2012, **85**, 053841/1.
12. K. Banerjee and G. Gangopadhyay, *J. Phys. B: At., Mol. Opt. Phys.*, 2012, **45**, 045102.
13. H. Fujisaki, *Phys. Rev. A*, 2004, **70**, 012313.
14. F. Spano and L. Silvestri, *J. Chem. Phys.*, 2010, **132**, 094704.
15. L. Zhai and Y. Zheng, *Int. J. Quantum Chem.*, 2014.
16. Z. Huang and S. Kais, *Chem. Phys. Lett.*, 2005, **413**, 1.
17. T. Juhász and D. A. Mazziotti, *J. Chem. Phys.*, 2006, **125**, 174105.
18. K. Boguslawski, P. Tecmer, G. Barcza, O. r. Legeza and M. Reiher, *J. Chem. Theory Comput.*, 2013, **9**, 2959.
19. T. S. Hofer, *Frontiers in chemistry*, 2013, **1**.
20. Z. Huang, H. Wang and S. Kais, *J. Mod. Opt.*, 2006, **53**, 2543.
21. S. Kais, *Adv. Chem. Phys.*, 2007, **134**, 493.
22. M. Lombardi and A. Matzkin, *Phys. Rev. A*, 2006, **73**, 062335.
23. T. Maiolo, D. Fabio, L. Martina and G. Soliani, *Quantum Computers and Computing*, 2006, **6**, 43.

24. T. A. Maiolo, F. Della Sala, L. Martina and G. Soliani, *Theoretical and Mathematical Physics*, 2007, **152**, 1146.
25. L. Martina and G. Soliani, *arXiv preprint arXiv:0704.3130*, 2007.
26. O. Osenda, P. Serra and S. Kais, *International Journal of Quantum Information*, 2008, **6**, 303.
27. A. Ramšak, I. Sega and J. Jefferson, *Phys. Rev. A*, 2006, **74**, 010304.
28. H. Wang and S. Kais, *Isr. J. Chem.*, 2007, **47**, 59.
29. M. D. Shulman, O. E. Dial, S. P. Harvey, H. Bluhm, V. Umansky and A. Yacoby, *Science*, 2012, **336**, 202.
30. T. Westermann and U. Manthe, *J. Chem. Phys.*, 2012, **136**, 204116.
31. T. Westermann and U. Manthe, *J. Chem. Phys.*, 2012, **137**, 22A509.
32. Z. Bihary, D. R. Glenn, D. A. Lidar and V. Ara Apkarian, *Chem. Phys. Lett.*, 2002, **360**, 459.
33. R. de Vivie-Riedle and U. Troppmann, *Chem. Rev.*, 2007, **107**, 5082.
34. T. Cheng and A. Brown, *J. Chem. Phys.*, 2006, **124**, 034111.
35. K. Mishima and K. Yamashita, *Int. J. Quantum Chem.*, 2009, **109**, 1827.
36. C. M. Tesch and R. de Vivie-Riedle, *Phys. Rev. Lett.*, 2002, **89**, 157901.
37. L. Zhai and Y. Zheng, *Phys. Rev. A*, 2013, **88**, 012504.
38. X.-W. Hou, J. Huang and M.-F. Wan, *Phys. Rev. A*, 2012, **85**, 044501.
39. X. W. Hou, M. F. Wan and Z. Q. Ma, *Opt. Commun.*, 2008, **281**, 3587.
40. X.-W. Hou, J. Huang and M.-F. Wan, *Phys. Rev. A: At., Mol., Opt. Phys.*, 2012, **85**, 044501/1.
41. F. Hai-Ran, M. Xiang-Jia, L. Peng and Z. Yu-Jun, *Chinese Physics B*, 2014, **23**, 073301.
42. K. Mishima, K. Shioya and K. Yamashita, *Chem. Phys. Lett.*, 2007, **442**, 58.
43. K. Mishima and K. Yamashita, *Chem. Phys.*, 2010, **367**, 63.
44. K. Mishima and K. Yamashita, *Chem. Phys.*, 2009, **361**, 106.
45. T. Yoshino, S. Nishida, K. Sato, S. Nakazawa, R. D. Rahimi, K. Toyota, D. Shiomi, Y. Morita, M. Kitagawa and T. Takui, *J. Phys. Chem. Lett.*, 2011, **2**, 449.
46. K. Sato, S. Nakazawa, R. Rahimi, T. Ise, S. Nishida, T. Yoshino, N. Mori, K. Toyota, D. Shiomi, Y. Yakiyama, Y. Morita, M. Kitagawa, K. Nakasuji, M. Nakahara, H. Hara, P. Carl, P. Hofer and T. Takui, *J. Mater. Chem.*, 2009, **19**, 3739.
47. K. Sato, R. Rahimi, N. Mori, S. Nishida, K. Toyota, D. Shiomi, Y. Morita, A. Ueda, S. Suzuki, K. Furukawa, T. Nakamura, M. Kitagawa, K. Nakasuji, M. Nakahara, H. Hara, P. Carl, P. Höfer and T. Takui, *Physica E: Low-dimensional Systems and Nanostructures*, 2007, **40**, 363.
48. R. Rahimi, K. Sato, K. Furukawa, K. Toyota, D. Shiomi, T. Nakamura, M. Kitagawa and T. Takui, *International Journal of Quantum Information*, 2005, **3**, 197.
49. K. Sato, S. Nakazawa, S. Nishida, R. Rahimi, T. Yoshino, Y. Morita, K. Toyota, D. Shiomi, M. Kitagawa and T. Takui, in *EPR of Free Radicals in Solids II*, eds. A. Lund and M. Shiotani, Springer Netherlands, 2012, vol. 25, pp. 163.
50. C. H. Bennett and D. P. DiVincenzo, *Nature*, 2000, **404**, 247.
51. K. H. Marti and M. Reiher, *Phys. Chem. Chem. Phys.*, 2011, **13**, 6750.
52. T. Yonehara, K. Hanasaki and K. Takatsuka, *Chem. Rev.*, 2012, **112**, 499.
53. J. C. Tully, *J. Chem. Phys.*, 2012, **137**, 22A301.
54. K. Takatsuka, *J. Phys. Chem. A*, 2007, **111**, 10196.
55. M. Born and R. Oppenheimer, *Ann. Phys.*, 1927, **84**, 0457.
56. M. Born, *Nachr. Akad. Wiss. Gottingen, Math.-physik. Klasse IIa, Math.-physik.-chem. Abt.*, 1951, 1.
57. T. Azumi and K. Matsuzaki, *Photochem. Photobiol.*, 1977, **25**, 315.
58. B. T. Sutcliffe and R. G. Woolley, *J. Chem. Phys.*, 2012, **137**, 22A544.
59. J. R. Reimers, L. McKemmish, R. H. McKenzie and N. S. Hush, *Phys. Chem.Chem. Phys.*, 2015, **submitted**, Paper 3.
60. K. Pae and V. Hizhnyakov, *J. Chem. Phys.*, 2013, **138**, 104103.
61. H. Rongsheng, L. Zijing and W. Kelin, *Physical Review B*, 2002, **65**, 174303.
62. E. B. D. Wilson, J. C; Cross, Paul C., *Molecular Vibrations: The Theory of Infrared and Raman Vibrational Spectra*, McGraw-Hill Book Company, New York, 1955.
63. J. R. Reimers, L. McKemmish, R. H. McKenzie and N. S. Hush, *Phys. Chem.Chem. Phys.*, 2015, **submitted**, Paper 1.
64. J. R. Reimers, L. McKemmish, R. H. McKenzie and N. S. Hush, *Phys. Chem.Chem. Phys.*, 2015, **submitted**, Paper 2.
65. Z.-L. Cai and J. R. Reimers, *J. Phys. Chem. A*, 2000, **104**, 8389.
66. J. F. Stanton, *J. Chem. Phys.*, 2010, **133**, 174309.
67. J. R. Reimers, B. B. Wallace and N. S. Hush, *Phil. Trans. Roy. Soc. A*, 2008, **366**, 15.
68. N. S. Hush, in *Mechanistic Aspects of Inorganic Reactions*, eds. D. B. Rorabacher and J. F. Endicott., 1982, vol. 198, pp. 301.
69. S. Woitellier, J. P. Launay and C. W. Spangler, *Inorg. Chem.*, 1989, **28**, 758.
70. J. R. Reimers and N. S. Hush, *Inorg. Chem.*, 1990, **29**, 3686.
71. J. R. Reimers and N. S. Hush, *J. Chem. Phys.*, 2003, **119**, 3262.
72. J. R. Reimers and N. S. Hush, *J. Am. Chem. Soc.*, 2004, **126**, 4132.
73. D. Curiel, K. Ohkubo, J. R. Reimers, S. Fukuzumi and M. J. Crossley, *Phys. Chem. Chem. Phys.*, 2007, **9**, 5260.
74. S.-H. Lee, A. G. Larsen, K. Ohkubo, Z.-L. Cai, J. R. Reimers, S. Fukuzumi and M. J. Crossley, *Chem. Sci.*, 2011, **3**, 257.
75. M. Brinkmann, G. Gadret, M. Muccini, C. Taliani, N. Masciocchi and A. Sironi, *J. Am. Chem. Soc.*, 2000, **122**, 5147.
76. S. Yin, L. Li, Y. Yang and J. R. Reimers, *J. Phys. Chem. C*, 2012, **116**, 14826.
77. M. Born and K. Huang, *Dynamical Theory of Crystal Lattices*, Clarendon, Oxford, 1954.
78. M. Reis, M. O. T. Cunha, A. C. Oliveira and M. C. Nemes, *Phys. Lett. A*, 2005, **344**, 164.
79. L. D. Landau, *Z. Phys. Sowjetunion*, 1932, **2**, 46.
80. C. Zener, *Proc. R. Soc. London, Ser. A*, 1932, **137**, 696.
81. M. D. Newton and N. Sutin, *Annu. Rev. Phys. Chem.*, 1984, **35**, 437.
82. D. N. Beratan and J. J. Hopfield, *J. Chem. Phys.*, 1984, **81**, 5753.
83. B. K. Kendrick, C. A. Mead and D. G. Truhlar, *Chem. Phys.*, 2002, **277**, 31.
84. A. W. Jasper, B. K. Kendrick, C. A. Mead and D. G. Truhlar, *Adv. Ser. Phys. Chem.*, 2004, **14**, 329.
85. P. T. Saunders, *An introduction to catastrophe theory*, Cambridge University Press, Cambridge, 1980.
86. F. Xu, *Z. Phys. Chem.*, 1990, **166**, 79.
87. X. Krokidis, B. Silvi, C. Dezarnaud-Dandine and A. Sevin, *New J. Chem.*, 1998, **22**, 1341.

Cite this: DOI: 10.1039/c0xx00000x

www.rsc.org/xxxxxx

ARTICLE TYPE

TOC graphic